JOURNAL OF MATERIALS SCIENCE 35 (2000) 1487–1494

Dielectric properties and crystal structure of $Ba_{6-3x}(Nd, M)_{8+2x}Ti_{18}O_{54}$ (M = La, Bi, Y) microwave ceramics

JEONG SEOG KIM, CHAE II CHEON
Department of Materials and Mechanical Engineering, Hoseo University, San 29-1, Sechul-ri, Baebang-myoun, Asan, Chungcheongnam-do, 336-795 Korea

TA-RYEONG PARK
Department of Physics, Hoseo University, Asan, Chungcheongnam-do, 336-795 Korea

HAE-SEOP SHIM
Department of Neutron Physics, Hanaro Center, KAERI, Taejon, 305-353 Korea

Crystal structure and dielectric property of tungsten-bronze type microwave dielectric ceramics, i.e., $BaOLa_2O_34TiO_2$ and $Ba_{6-3x}(Nd, M)d_{8+2x}Ti_{18}O_{54}$ (M = Y, Bi and $x = 0.5, 0.7$), are analysed. The optimum properties obtained in $Ba(Nd_{1-x}Bi_x)_2O_34TiO_2$ were $\varepsilon_r = 89$–92, $Qf = 5855$–6091 GHz, and $\tau_f = -7$–$+7$ ppm/°C $x = 0.04$–0.08. The Y-substitution in $BaO(Nd_{1-x}Y_x)_2O_34TiO_2$ reduces the dielectric constant ε_r. Both the Y and Bi substitutions make $\tau_{\varepsilon r}$ positive. The relative dielectric constant ε_r and temperature coefficient $\tau_{\varepsilon r}$ are 109.5 and -180 ppm/°C in $BaOLa_2O_34TiO_2$, 76 and $+40$ ppm/°C in $BaO(Nd_{0.77}Y_{0.23})_2O_34TiO_2$, respectively. The crystal structures were refined by Rietveld method using x-ray and neutron diffraction data. The most reliable results were obtained by refining the cation positions using the x-ray data and the oxygens from the neutron with a superlattice structure model Pnam(*c*-axis ≈7.6 Å). The refined structures show that the a/c ratios are related to the apical oxygen displacements of the Ti–O octahedra. The substitution of the small radius atom, Y, produced a structure of severely tilted and distorted Ti–O octahedra and large a/c ratio, while the large radius atom, La, small a/c ratio. Differential scanning calorimetry analysis showed heat anomaly indicating suspected phase transition in these materials. The relation between $\tau_{\varepsilon r}$ and octahedron tilting in tungsten-bronze type material is discussed in relation with complex perovskite structure. © *2000 Kluwer Academic Publishers*

1. Introduction

Dielectric ceramics in BaO-R_2O_3-TiO_2 (R = rare earth) ternary system have been commercially utilized as microwave ceramic resonators as well as ceramic capacitors [1, 2]. In spite of the practical importance of this dielectric ceramic, the crystal structural characteristics have not been known clearly even with many studies reported concerning the BaO-Nd_2O_3-TiO_2 system. Lately Ohsato *et al.* [3] reported that the dielectric ceramics form the Ba_{6-3x} $R_{8+2x}Ti_{18}O_{54}$ (R = rare earth) solid solution. The $BaONd_2O_34TiO_2$ ceramics reported by Takahashi *et al.* [4] and the $Ba_{3.75}Pr_{9.5}Ti_{18}O_{54}$ reported by Mateeva *et al.* [5] correspond exactly to $x = 0.5$ and 0.75 of the solid solution compounds, respectively. The other ceramic compositions, such as $BaONd_2O_35TiO_2$ and $4BaO5Nd_2O_318TiO_2$ [6, 7] slightly deviate from the solid solution formula.

The crystal structure refinement with fundamental lattice model of Pba2 space group was originally done by Mateeva *et al.* [5] for the $Ba_{3.75}Pr_{9.5}Ti_{18}O_{54}$. The crystal structure is a tungsten bronze-type with 2×3 perovskite blocks and pentagonal channels formed by the infinite Ti–O octahedron chains along the *c*-axis. Mateeva *et al.*'s refinement has been provided the basic understandings of the crystal structure until now, even though considerable ambiguities remained in the refinement results which will be discussed in this paper. Recently, Azough *et al.* [8] tried a structural refinement using the superlattice model with Pnam space group derived from transmission electron diffraction work. However, their results was not successful due to that the atomic positions and other atomic variables were incorrectly set for the structure refinement by Rietveld method.

The dielectric properties of the BaO-R_2O_3-TiO_2 ceramics, especially the temperature coefficient of dielectric constant $\tau_{\varepsilon r}$, critically depends on the composition and the additives. Early works include the substitutions of Pr_2O_3, Sm_2O_3, Gd_2O_3, and La_2O_3 for the Nd_2O_3 and the addition of small amount additives, such as WO_3, MnO, SrO, Bi_2O_3 and PbO [8–11]. The Bi_2O_3 addition reported to narrow down the temperature

coefficient of resonant frequency τ_f to 0–10 ppm/°C in the BaO-Nd_2O_3-TiO_2 ceramics. Durand and Boilot [12] added 10 wt% $2Bi_2O_33TiO_2$ to $BaONd_2O_34TiO_2$ to produce the τ_f of 8 ppm/°C. Wersing [13] improved the τ_f to 10 ppm/°C by substituting small amount of Bi_2O_3 for the TiO_2 in the $BaONd_2O_35TiO_2$. However, these reports did not clearly show for which sites the Bi substitutes in the $Ba_{6-3x}R_{8+2x}Ti_{18}O_{54}$. Mizuta *et al.* [14] reported in $(Ba_{6-3x}Sn_{8+2x})_\alpha Ti_{18-y}Al_yO_{54}$ ($\alpha = 1 + y/36$) that τ_f decreased to negative value with increase of x and/or y, and the structural change of Ti-O octahedron tilting was suggested for the τ_f change. However, any detailed explanation to the $\tau_{\varepsilon r}$ or τ_f change with the substitution of varying elements has not been given due to the complexity of the crystal structure.

In this study, the effect of ionic size of substitution atom on the dielectric properties and crystal structure were systematically investigated: The ionic radii (A-IR) of the substitutes, Y, Bi, Nd, and La are 0.92, 0.96, 1.04, 1.14 Å, respectively [15]. Especially, the relation between $\tau_{\varepsilon r}$ and Ti–O octahedron tilting observed in the tungsten-bronze type structure is discussed in relation with complex perovskite materials. This study also reports a suspected phase transition phenomenon in the $Ba_{6-3x}Re_{8+2x}Ti_{18}O_{54}$ observed by DSC analysis. The crystal structures are analysed using Rietveld refinement method in relation with the dielectric properties.

2. Experimental procedure

Starting materials were high purity $BaCO_3$, TiO_2, Bi_2O_3, Y_2O_3, La_2O_3 and Nd_2O_3. The powders were weighed in appropriate ratios to yield following samples:

– $Ba_{6-3x}Nd_{8+2x}Ti_{18}O_{54}$ [BNT: $x = 0.5$, BNV: $x = 0.7$]
– $BaO[(Nd_{1-x}Bi_x)_2O_3]4TiO_2$ [$x = 0$–0.2, B(NB)T: $x = 0.09$]
– $BaO[(Nd_{1-x}Y_x)_2O_3]4TiO_2$ [$x = 0$–0.3, B(NY)T: $x = 0.23$]
– $BaOLa_2O_34TiO_2$ [BLT]

Each batches of powder was ball milled for 20 hours, calcined at 1000°C for 3 hours, and then ball-milled again for 15 hours with 1 wt% PVA. The resulting slurries were dried and pressed at 1 ton/cm^2 into pellets of 12 mm diameter and thickness of 1–5 mm. The pressed pellets were sintered at 1320–1360°C for 2 hours in air. Dielectric properties were measured either at 4.5–5.2 GHz using a network analyzer (Hakki Coleman method [16]) or at 1 MHz using impedance analyzer (HP4192A). Temperature coefficient of resonance frequency τ_f was calculated using the following equation.

$$\tau_f = -\frac{\tau_{\varepsilon r}}{2} - \alpha_i \qquad (1)$$

where $\tau_{\varepsilon r}$ and α_i are the temperature coefficients of relative dielectric constant measured at 1 MHz and thermal expansion coefficient of the material ($\approx 10^{-5}$/K) respectively [13]. Sintered densities were measured by Archimedes method.

The x-ray powder diffraction data for the Rietveld analysis were collected using the Rigaku Dmax-100 diffractometer with parameters as followings: diffracted beam monochromator, Cu K_α radiation, 40 kV-40 mA, 0.04° step-scan, 2 sec fixed time at each step, iteration = 2 (or 1) and slits of DS = 1.0° (or 2.0°), SS = 1.0°, RS = 0.15 mm. The data collection angle 2θ was in the range of 15–80°. Neutron powder diffraction data of the samples were obtained at room temperature using the high-resolution powder diffractometer HRPD at KAERI (Korea Atomic Energy Research Institute). Neutrons from the ST2 channel of the reactor HANARO was monochromatized by a vertically focusing composite Ge monochromator at 90 degree take-off position to a wavelength of 0.18339 nm. The data was collected in the range of 0 to 160 degree and 0.05 deg/step with about a 10 g sample in a vanadium can which was supported in the neutron beam on a rotating cadmium rod to minimize any preferred orientation effect in the powder and signal-to-noise ratio. The Rietveld refinements were performed using DBWS 9411 for the x-ray data and Full-prof for the neutron data.

3. Results and discussion

3.1. Crystal structure

Rietveld analyses have been carried out on the several samples: BNT, BNV, B(NB)T, B(NY)T, and BLT. Both the fundamental lattice with space group Pbam and the superlattice with Pnam model were tested for the crystal structure refinement. The fundamental lattice model followed Mateeva *et al.*'s [5] results. The superlattice parameters and the space group are based on the transmission electron diffraction reported by Azough *et al.* [8] and x-ray single crystal diffraction work by Ohsato *et al.* [10]. In the latter work, only the lattice parameter and the space group were provided without structure refinement.

The refinement results on the B(NB)T and that of Mateeva *et al.*'s results on $Ba_{3.75}Pr_{9.5}Ti_{18}O_{54}$ [5] using x-ray data and the fundamental lattice model Pbam are shown in Table I. Some Ti–O bond lengths are found in the range of 1.5–1.7 Å which are extraordinarily short for the normal Ti-O bond length of 1.8–2.0 Å. This false result is ascribed to the improper space group or incorrectly refined oxygen positions due to small scattering factor of oxygen compared to the cations. The superlattice structure with doubled c-axis parameters was tested using Pnam space group for BLT and B(NY)T. In Tables II–V are summarized the refinement results. In Table II the refined lattice parameters and a/c ratios are shown with ceramic compositions. In Table III "goodness of fitness χ" and "R-factors" are compared for the two samples obtained from the x-ray, neutron, "combined" method. The "combined" method implies the refinement of the cation positions from the x-ray data and the oxygen positions by neutron data. The χ and R-factors from the x-ray data were relatively high compared to the neutron and "combined" method. Table IV shows the positional, thermal, and occupational parameters by the "combined method" of BLT.

TABLE I Summary of structural refinement; some selected bond lengths are compared to Mateeva *et al.*'s results

Composition	$Ba_{3.75}Pr_{9.5}Ti_{18}O_{54}$[a]	B(NB)T[$(0.91Nd_2O_3 0.09Bi_2O_3)$]
Rp, Rwp, S[b], space group	9.0, –, –, Pba2	7.57, 10.13, 2.01, Pbam
a, *b*, *c* (Å)	22.360, 12.181, 3.832	22.306, 12.177, 3.835
Ti—O bond lengths[c]		
Ti1 –O8, –O8	1.567, 2.265	1.924, 1.924
–2O9, –2O11	1.944, 1.988	1.988, 1.764
Ti2 –O5, –O6	2.061, 1.813	2.047, 1.970
–O6, –O10	2.091, 1.831	1.970, 1.594
–O11, –O1	2.061, 1.870	2.209, 1.959
Ti4 –O1, –O1	1.894, 1.984	1.945, 1.945
–O3, –O7	1.869, 1.911	1.856, 2.046
–O9, –O13	2.129, 1.945	1.920, 2.206
Ti5 –O2, –O3	1.832, 2.010	1.919, 1.889
–O4, –O4	1.718, 2.184	2.008, 2.008
–O10, –O13	2.387, 1.915	2.692, 1.701

[a]Calculated from Mateeva *et al.*'s atomic parameters.
[b]Goodness of fitness.
[c]Atomic notation followed the Mateeva *et al.*'s atomic parameters.

TABLE II Lattice parameter (Å), a/c ratio, and transition temperatures with composition change in $Ba_{6-3x}Nd_{8+2x}Ti_{18}O_{54}$

Composition	*a*	*b*	*c*	a/c	T_c (°C)[a]
$Ba_{4.5}Nd_9Ti_{18}O_{54}$					
BNT ($x = 0.5$)	22.3294	12.1964	7.6924	2.903	291
$Ba_{3.9}Nd_{9.4}Ti_{18}O_{54}$					
BNV ($x = 0.7$)	22.3088	12.1783	7.6716	2.908	295
$0.77Nd_2O_3 0.23Y_2O_3$					
B(NY)T ($x = 0.5$)	22.2988	12.1462	7.6616	2.910	310
$0.91Nd_2O_3 0.09Bi_2O_3$					
B(NB)T ($x = 0.5$)	22.3364	12.1982	7.6985	2.901	282
BLT	22.4123	12.2777	7.7526	2.8909	—

[a]Measured by DSC.

TABLE III Refined R-factors from the x-ray, neutron, and "combined"

	BLT				B(NY)T			
'R'	*R*p	*R*wp	*R*b	χ^2	*R*p	*R*wp	*R*b	χ^2
X-ray	7.37	9.59	3.99	3.39	7.10	9.84	4.99	9.18
Neutron	5.10	6.65	4.35	1.68	4.83	6.32	4.94	1.90
Combined	5.47	7.20	5.17	1.96	5.42	7.11	6.48	2.38

TABLE IV Positional and thermal parameters refined by the "combined" method of $BaOLa_2O_3 4TiO_2$

Atoms	*x*	*y*	*z*	*B*	Occup.
Ba1	0.3106	0.0944	0.2500	0.507	0.513(20)
Ba2	0.8042	0.4086	0.7500	0.518	0.485(20)
La1	0.0540	0.2058	0.2500	0.524	0.425(13)
La2	0.4538	0.7008	0.2500	0.524	0.453(14)
La3	0.4980	0.0009	0.2500	0.524	0.442(7)
La4	0.3800	0.4028	0.2500	0.524	0.453(12)
La5	0.6192	0.5907	0.2500	0.524	0.462(13)
Ti1	0.5000	0.5000	0.0000	1.360(96)	0.500
Ti2	0.4349	0.1984	−0.0070	1.360(96)	1.000
Ti3	0.1105	0.3976	0.0039	1.360(96)	1.000
Ti4	0.1646	0.1138	0.0116	1.360(96)	1.000
Ti5	0.2620	0.3367	0.0142	1.360(96)	1.000
O1	0.1656(6)	0.1035(13)	0.2500	1.063(44)	0.500
O2	0.1452(6)	0.0944(13)	0.7500	1.063(44)	0.500
O3	0.1943(3)	0.4199(6)	0.0038(23)	1.063(44)	1.000
O4	0.2395(3)	0.1839(6)	−0.0181(18)	1.063(44)	1.000
O5	0.2748(8)	0.3200(17)	0.2500	1.063(44)	0.500
O6	0.2733(7)	0.3297(17)	0.7500	1.063(44)	0.500
O7	0.0209(4)	0.3646(6)	−0.0025(20)	1.063(44)	1.000
O8	0.4479(7)	0.2182(11)	0.2500	1.063(44)	0.500
O9	0.4390(7)	0.1864(12)	0.7500	1.063(44)	0.500
O10	0.1172(3)	0.2432(7)	0.0099(17)	1.063(44)	1.000
O11	0.4860(7)	0.4885(13)	0.2500	1.063(44)	0.500
O12	0.0787(3)	0.0469(7)	0.0316(14)	1.063(44)	1.000
O13	0.3602(3)	0.2628(6)	−0.0068(20)	1.063(44)	1.000
O14	0.4728(4)	0.3470(7)	−0.0314(14)	1.063(44)	1.000
O15	0.4052(4)	0.0508(6)	0.0325(16)	1.063(44)	1.000
O16	0.3118(3)	0.4656(2)	0.0074(20)	1.063(44)	1.000
O17	0.1006(6)	0.4135(12)	0.2500	1.063(44)	0.500
O18	0.1031(7)	0.3859(13)	0.7500	1.063(44)	0.500

The full occupancies of Ba and La sites are 0.5. The occupancies of La sites in the range of 0.425–0.462 imply partially vacant by about 10%, which is expected from the chemical formula $Ba_{6-3x}La_{8+2x}Ti_{18}O_{54}$. At $x = 0$, Ba and La sites are fully occupied and with increasing x becomes partially vacant to make charge balance.

In Table V the credibility of the refined positional parameters of Table IV are tested by applying "the valence sum rule" and the "bond valences" [17] for each atoms and calculated using following equation.

$$BV_i = \sum_j S_{ij} = \sum \exp\left(\frac{r'_o - r_{ij}}{B}\right) \qquad (2)$$

where, BV_i is bond valence of ith ion, r'_o experimental and calculated bond distances of each ions, B constant with 0.37, r_{ij} refined ionic distance between the i and j atoms. The $r1$ of the "global instability index" $\langle r1\rangle$rms in Table V means $(\Sigma_j S_{ij} - V_i)$ and indicates the deviation parameters of the bond valence $\Sigma_j S_{ij}$ from the formal valence V_i. The refinement results with low value of $\langle r1\rangle$rms imply high reliability. Therefore the result by the "combined" method with the smallest value is the most reliable. For the case of the neutron, B(NY)T showed the largest value of $\langle r1\rangle$rms while that of BLT was smaller than x-ray as shown in Table V. The most reliable result from the "combined" is ascribed to that the x-ray provides an advantage for the cation position

TABLE V Calculated bond valences of $BaOLa_2O_34TiO_2$ and $BaO(Nd_{0.77}Y_{0.23})_2O_34TiO_2$

	$BaO(Nd_{0.77}Y_{0.23})_2O_34TiO_2$			$BaOLa_2O_34TiO_2$		
Atom	X-ray	Neutron	Combined	X-ray	Neutron	Combined
Ba1	2.57	2.98(10)	2.25(4)	2.51	1.93(3)	2.03(2)
Ba2	2.11	2.42(5)	1.87(3)	1.54	2.15(4)	2.19(3)
La1	4.42	3.49(9)	2.86(4)	3.29	2.90(4)	3.10(4)
La2	2.38	4.25(12)	3.48(6)	2.56	2.99(5)	3.14(3)
La3	3.34	3.77(9)	3.02(5)	2.43	2.79(4)	2.79(3)
La4	3.45	3.65(9)	2.91(5)	3.25	2.68(4)	2.98(4)
La5	3.15	3.57(9)	3.02(5)	2.26	3.04(5)	2.96(3)
Ti1	5.23	5.20(8)	4.17(6)	4.72	4.04(4)	4.18(4)
Ti2	3.40	4.93(17)	3.92(5)	3.97	3.97(9)	3.93(3)
Ti3	4.32	5.11(17)	3.99(5)	4.46	4.21(9)	4.11(3)
Ti4	4.18	5.13(16)	4.13(6)	3.84	3.94(9)	4.10(3)
Ti5	3.53	4.87(17)	4.04(9)	3.83	3.64(8)	3.86(3)
O1	2.10	2.18(10)	1.91(3)	2.34	1.79(6)	2.27(2)
O2	1.77	2.80(12)	1.97(4)	1.49	2.08(7)	1.71(2)
O3	2.32	2.46(10)	2.19(6)	2.09	2.00(5)	2.11(3)
O4	2.14	3.08(12)	2.24(6)	2.21	2.11(5)	2.10(3)
O5	2.13	2.94(15)	2.03(4)	2.28	1.45(5)	2.24(2)
O6	1.71	1.74(9)	1.66(3)	1.36	2.13(7)	1.43(2)
O7	1.99	2.39(8)	1.87(4)	1.77	1.82(4)	1.82(2)
O8	1.80	2.23(10)	1.79(3)	1.72	1.74(5)	1.75(2)
O9	2.15	2.96(16)	2.12(3)	2.12	2.29(9)	2.13(1)
O10	2.25	3.32(14)	2.21(5)	2.13	2.25(6)	2.25(3)
O11	2.04	2.45(5)	1.93(3)	1.99	2.03(3)	1.97(2)
O12	2.13	2.35(7)	2.03(4)	1.97	2.01(3)	2.04(2)
O13	2.65	2.43(7)	2.13(4)	2.10	1.92(5)	1.80(2)
O14	2.01	2.43(7)	1.75(4)	1.83	1.87(4)	1.96(3)
O15	2.09	2.06(9)	2.07(4)	2.00	1.87(5)	1.98(2)
O16	2.22	2.53(10)	2.08(6)	2.23	2.05(5)	2.12(2)
O17	1.98	2.20(9)	1.91(3)	2.19	1.41(4)	2.05(2)
O18	2.13	2.65(12)	2.10(3)	1.78	2.70(8)	1.83(2)
$\langle$r1$\rangle$rms[a]	**0.445**	**0.753**	**0.169**	**0.352**	**0.249**	**0.184**

[a]Global instability parameters $\langle r1\rangle$rms (rms: root mean square).

refinement, while the neutron does for the oxygen position due to large scattering power for oxygen. The calculated bond lengths from the refined structure of B(NY)T by the x-ray, neutron, and "combined" methods show that both in the x-ray and neutron results some bond lengths with smaller than 1.8 Å are found which is abnormally small for Ti–O bond, while in the "combined" all the bond lengths are larger than 1.8 Å. The calculated Ti–O bond lengths from the refined structure also imply that the "combined" method is the most reliable one.

Fig. 1 shows the refined crystal structure of BLT. The doubling of *c*-axis can be seen to be produced by the Ti–O octahedron distortion and consequent displacements of cations, La and Ba, in *x*-*y* plane.

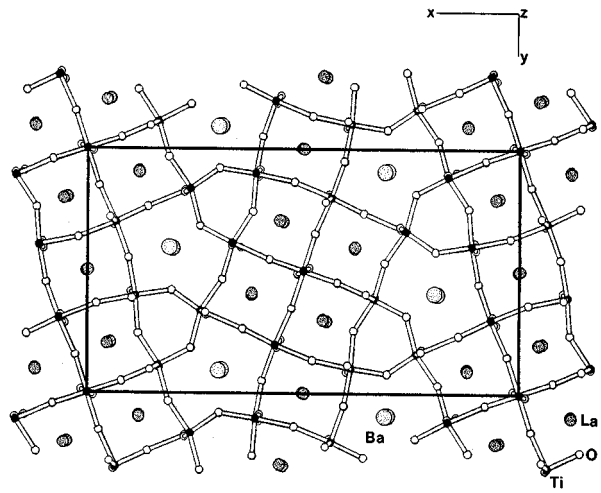

Figure 1 Refined crystal structure of the BLT with a superlattice structure.

3.2. Physical properties

X-ray powder diffraction analyses on the specimens, $Ba_{6-3x}Nd_{8+2x}Ti_{18}O_{54}$ [$x = 0.5$, $x = 0.7$] and $BaO[(Nd_{1-x}Bi_x)_2O_3]4TiO_2$ [$x = 0$–0.2] showed a single phase pattern. Fig. 2 shows the variation of apparent densities of $BaO(Nd_{1-x}Bi_x)_2O_34TiO_2$ sintered at 1340°C for 2 hours. The density increased steeply with the addition of Bi until $x = 0.04$. The ε_r and Qf of $BaO(Nd_{1-x}Bi_x)_2O_34TiO_2$ are shown in Fig. 3. The ε_r increased continuously with increasing Bi-substitution. Qf (GHz) showed a maximum at $x = 0.04$ and decreased with $x > 0.04$. The effect of Bi-substitution on $\tau_{\varepsilon r}$ and τ_f are shown in Fig. 4. The $\tau_{\varepsilon r}$ approaches to near zero at $x = 0.08$, and changes to positive values with further increasing x. The τ_f was calculated based on the measured $\tau_{\varepsilon r}$ using the equation 1.

With Y_2O_3 substitution dielectric constant ε_r decreases and reaches a minimum at $x = 0.15$ as shown in Table VI. The $\tau_{\varepsilon r}$ is +14 ppm/°C at $x = 0.23$. The loss factor increases with x and the solubility limit is

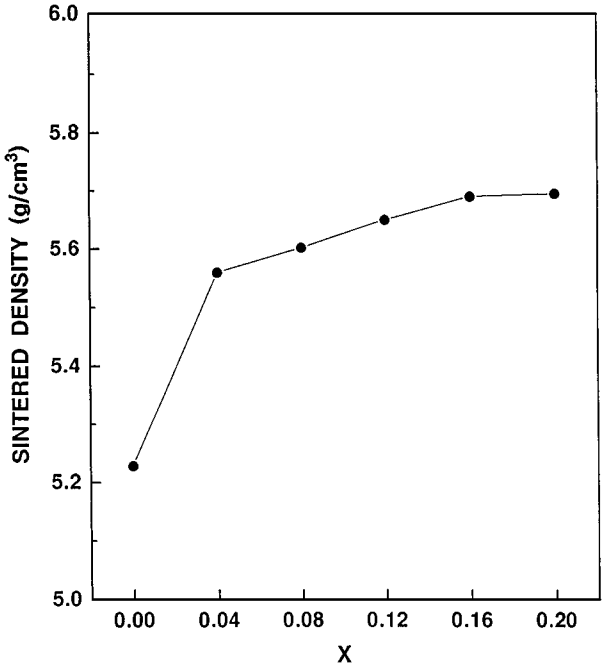

Figure 2 Variation of sintered densities of $BaO(Nd_{1-x}Bi_x)_2O_34TiO_2$ at 1340°C for 2 hours.

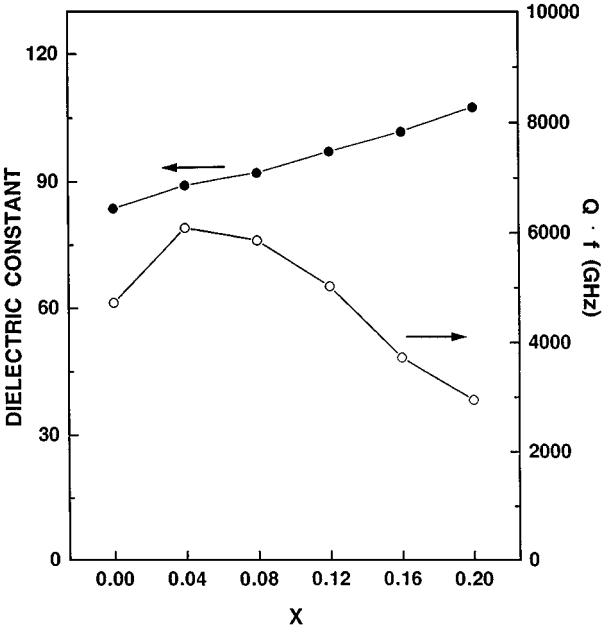

Figure 3 Dielectric properties of $BaO(Nd_{1-x}Bi_x)_2O_34TiO_2$ sintered at 1340°C for 2 hours.

$x \approx 0.23$. At $x = 0.3$, the XRD pattern showed an impurity phase $Y_2Ti_2O_7$. There is some discrepancy in ε_r values of the BNT between that in Table VI and in Fig. 3. This discrepancy is ascribed to the differences in the $\tau_{\varepsilon r}$ measurement chamber used. The BLT with large ionic size substitute has large ε_r and negative $\tau_{\varepsilon r}$.

In the $Ba_{6-3x}Nd_{8+2x}Ti_{18}O_{54}$ a phase transition can affect the $\tau_{\varepsilon r}$ as suggested by Wersing *et al.* The phase transition was analysed using differential scanning calorimetry (DSC), Dupont 2100 model, at a heating rate of 3 °C/min in the temperature range up to 500°C. Four samples i.e., B(NB)T, BNT, BNV and B(NY)T were tested. The results are shown in Fig. 5. Each samples was run for two times and showed the same results. In the B(NY)T a heat anomaly indicating phase transition clearly appears at about 310°C. The heat anomalies of the B(NB)T, BNT and BNV are also observed at 282 °C, 291 °C and 295 °C, respectively. The strong heat anomaly of the B(NY)T indicates the structural change is a first order transition characteristic. And those of the B(NB)T, BNV, and BNT with relatively small are more of second order characteristic than the B(NY)T. The measured phase transition temperature T_c is considered to be related with the a/c values shown in Table II. The T_c increases with a/c ratio increase by the substitution of small radius atom, Y, while the T_c decreases with the a/c decrease by the Bi-substitution. However, the transition temperatures are considered to be rather high to affect the $\tau_{\varepsilon r}$. Further study is needed for the nature of the suspected phase transition. The variation of $\tau_{\varepsilon r}$ with the ionic radius of the substitutes will be discussed in relation to the crystal structure.

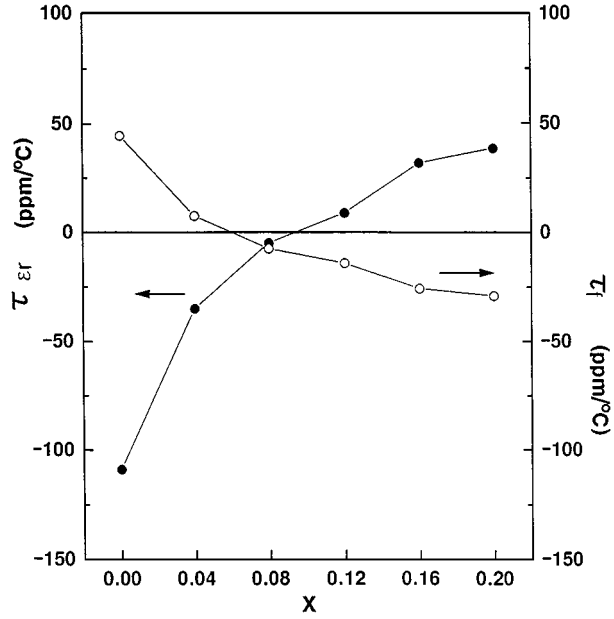

Figure 4 Temperature coefficients of dielectric constant $\tau_{\varepsilon r}$ and resonance frequency τ_f of the materials in Fig. 3.

3.3. Relation between physical properties and crystal structure

In $Ba_{6-3x}R_{8+2x}Ti_{18}O_{54}$ ceramics, any appropriate rationale has not been known for the change of τ_f with ceramic compositions. Wersing [13] found some dielectrics, such as $LaAlO_3$, $SrZrO_3$, $BaO\text{-}Nd_2O_3\text{-}TiO_2$ ceramics to deviates from the theoretically predicted relation between $\tau_{\varepsilon r}$ and ε_r for non-ferroelectric perovskites, which is represented as $\tau_{\varepsilon_r} \approx -\alpha_i \varepsilon_r$. A structural phase transition was assumed and suggested as the reason for the deviation. Concerning the relation between the crystal structure and τ_f, Ohsato *et al.* suggested that Ti–O octahedral shrinkage by vacancy increase with x in $Ba_{6-3x}Sm_{8+2x}Ti_{18}O_{54}$ ($0.3 \leq x \leq 0.7$) can give rise to negative τ_f value. And Mizuta *et al.* [14] also suggested Ti–O octahedron tilting by the cation substitution y in $(Ba_{6-3x}Sm_{8+2x})_\alpha Ti_{18-y}Al_yO_{54}$ ($\alpha = 1 + y/36$) can change τ_f to negative value.

TABLE VI Dielectric properties of $BaO(Nd_{1-x}Y_x)_2O_34TiO_2$ and $BaOLa_2O_34TiO_2$

Composition	ε_r	$\tau_{\varepsilon r}$ (ppm/°C)	tan δ	Phase
$BaO(Nd_{1-x}Y_x)_2O_34TiO_2$				
$x = 0$ (BNT)	99.8	−95	3×10^{-4}	Single phase
$x = 0.15$	85.0	−43	1×10^{-3}	Single phase
$x = 0.23$	89.8	+14	2×10^{-3}	Single phase
$x = 0.3$	93.6	+165	2×10^{-3}	$Y_2Ti_2O_7$ impurity
$BaOLa_2O_34TiO_2$ (BLT)	109.5	−180	5×10^{-4}	Single phase

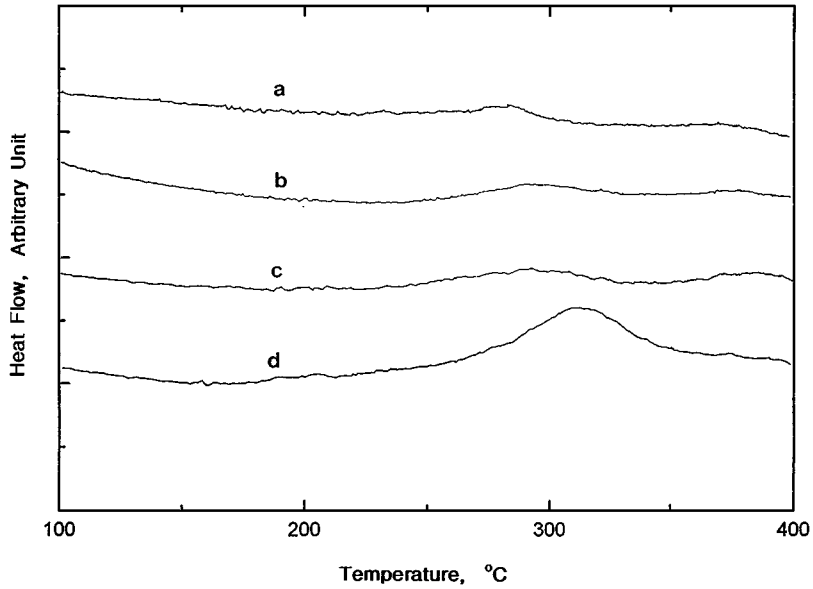

Figure 5 Differential scanning calorimetry (DSC) analysis results of the B(NB)T (a), BNT (b), BNV (c), and $BaO((Nd_{0.77}Y_{0.23})_2O_3)4TiO_2$(d).

The relation between $\tau_{\varepsilon r}$ and Ti–O octahedron tilting in the complex perovskite had been reported by Reaney *et al.* [18]. In this report, $\tau_{\varepsilon r}$ decreased with decrease of 'tolerance factor' t in 'no-tilting' region of perovskite structure, and reaches a minimum in 'antiphase tilting' region. With further decrease of t, $\tau_{\varepsilon r}$ increases and reaches a maximum in the '3-tilt' system region with 'in-phase' and 'anti-phase' tiltings. Since the perovskite blocks are mainly consisted in the crystal structure of the tungsten-bronze type, the relation between $\tau_{\varepsilon r}$ and Ti–O octahedron tilting found in complex perovskite would be applicable to the tungsten bronze system.

In Fig. 6 are shown some selected Ti–O bonds depicting octahedron tilting and distortion. The tilting mode in this tungsten bronze structure does not simply follow Glazer's model [19] for complex perovskite. The apical oxygens indicated by arrows coordinating Ti5 (i.e., O4, O16, O5, O6), Ti2(i.e., O8, O9, O14, O15), and Ti3 (i.e., O17, O10, O15) can be seen to be substantially displaced in the direction of the arrows. This type of cooperative oxygen displacements, consequently, increases the bond lengths of Ti5–O13, Ti2–O7, Ti3–O7 while reduces those of Ti5–O3, Ti2–O13, Ti3–O3 bond lengths due to the electrical repulsion induced by the oxygen displacements as indicated by arrows. The reduced and lengthened bond lengths by these displacements are shown in Table VII.

These cooperative oxygen displacements give rise to the "crumpled" Ti–O octahedron structure, and reduce the c-axis length compared to untilted perovskite

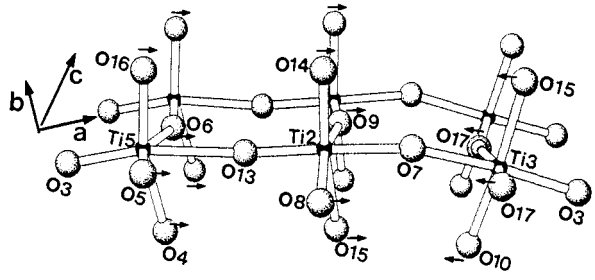

Figure 6 Selected Ti–O octahedra from Fig. 1 depicting the oxygen displacements and bond angles.

TABLE VII Some selected bond lengths of BLT and B(NY)T refined by "combined" method

Bond type	$BaOLa_2O_34TiO_2$	$BaO(Nd_{0.77}Y_{0.23})_2O_34TiO_2$
Ti5–O3	1.8305(79)	1.8149(201)
Ti5–O13	2.3867(84)	2.3853(196)
Ti2–O7	2.0785(93)	2.0455(148)
Ti2–O13	1.8513(83)	1.8873(125)
Ti3–O3	1.8987(81)	1.9000(134)
Ti3–O7	2.0479(94)	2.0613(152)

structure. The distortion mode of oxygen octahedra both in BLT and B(NY) is similar. Most significant difference in the two crystal structures is found in the extent of octahedron tiltings and distortion i.e., bond angles of Ti—O—Ti and O—Ti—O. In Table VIII are shown the bond angles of O—Ti—O. Except some O—Ti—O bonds (marked with *) existing intimately near Ba-filled pentagon-channels where the periodicity of Ti—O octahedra arrangement are interrupted, all the O—Ti—O angles decrease with the ceramic composition change from BLT to B(NY)T as shown in Table VIII. Table IX shows the bond angles of Ti—O—Ti indicating the extent of octahedron tilt. The larger the deviation from 180° the larger the tilting of octahedra. All the Ti—O—Ti bond angles are smaller in B(NY)T than BLT except some Ti—O—Ti bonds (marked with *) existing near the pentagon channels similarly to the O—Ti—O bonds.

TABLE VIII Bond angles in Ti—O6 octahedrons of $BaOLa_2O_34TiO_2$ and $BaO(Nd_{0.77}Y_{0.23})_2O_34TiO_2$

	Bond angle (degree)	
Bond type	$BaOLa_2O_34TiO_2$	$BaO(Nd_{0.77}Y_{0.23})_2O_34TiO_2$
O11—Ti1—O11	179.97(26)	179.97(47)
O12—Ti1—O12	180.00(80)	179.97(14)
O14—Ti1—O14	180.00(89)	180.00(13)
O7—Ti2—O13	176.46(82)	176.21(13)
O8—Ti2—O9	168.62(17)	163.36(34)
O14—Ti2—O15	173.92(83)	171.90(12)
O3—Ti3—O7	176.54(80)	167.75(13)
[a]*O10—Ti3—O15*	*170.76(82)*	*173.41(12)*
O17—Ti3—O18	168.53(14)	167.10(31)
O1—Ti4—O2	164.61(18)	164.41(39)
O4—Ti4—O12	175.13(77)	166.89(12)
[a]*O10—Ti4—O16*	*161.82(67)*	*163.32(14)*
O3—Ti5—O13	166.70(71)	166.37(13)
[a]*O4—Ti5—O16*	*158.02(64)*	*161.00(16)*
O5—Ti5—O6	161.76(14)	156.85(33)

[a]Italic letters: O—Ti—O bonds around the pentagon-channels in *a-b* plane.

TABLE IX Selected tilt angles of Ti-O6 octahedrons of $BaOLa_2O_34TiO_2$ and $BaO(Nd_{0.77}Y_{0.23})_2O_34TiO_2$

	Angle (degree)	
Bond type	$BaOLa_2O_34TiO_2$	$BaO(Nd_{0.77}Y_{0.23})_2O_34TiO_2$
Ti1—O11—Ti1	159.95(12)	154.22(21)
Ti1—O14—Ti2	165.77(40)	158.99(56)
Ti1—O12—Ti4	167.21(34)	155.18(57)
Ti2—O9—Ti2	169.41(6)	165.74(13)
Ti2—O8—Ti2	158.42(12)	149.22(23)
Ti2—O15—Ti3	160.14(35)	156.99(54)
Ti3—O17—Ti3	162.39(10)	162.01(14)
Ti3—O18—Ti3	167.31(7)	158.36(20)
Ti3—O10—Ti4	150.81(38)	149.31(57)
[a]*Ti3—O3—Ti5*	*137.67(35)*	*138.75(115)*
Ti4—O1—Ti4	172.07(5)	163.42(14)
[a]*Ti4—O4—Ti5*	*130.25(37)*	*135.57(117)*
[a]*Ti4—O16—Ti5*	*160.78(21)*	*161.69(125)*
Ti5—O5—Ti5	158.01(16)	152.50(49)
Ti5—O6—Ti5	165.16(9)	159.32(42)

[a]Italic letters: Ti—O—Ti tilted bonds lying in *a-b* plane around the pentagon-channels.

Therefore, the bond angle changes in Tables VIII and IX show that the octahedra in the B(NY)T are more severely tilted and distorted.

Colla *et al.* [18] derived an expression for $\tau_{\varepsilon r}$ at constant pressure as following:

$$\tau_{\varepsilon r} = \frac{(\varepsilon-1)(\varepsilon+2)}{3\varepsilon}\left[\frac{1}{\alpha m}\left(\frac{\partial \alpha m}{\partial T}\right)_v + \frac{1}{\alpha m}\left(\frac{\partial \alpha m}{\partial v}\right)_T\left(\frac{\partial v}{\partial T}\right)_P - \frac{1}{v}\left(\frac{\partial v}{\partial T}\right)_P\right] \quad (3)$$

where αm is polarizability, v volume, and ε_r relative dielectric constant. The first term in the bracket in Equation (3) is related with crystal structure and normally has negative value. With more severely tilted octahedron structure, this term becomes less important and $\tau_{\varepsilon r}$ depends mainly on the last two terms. Hence perovskite ceramics with small A-site cations tend to have near zero or positive $\tau_{\varepsilon r}$. Both the BLT and B(NY)T have tilted and distorted octahedra as discussed previously, and B(NY)T with small rare earth atoms, Nd and Y, is more severely tilted than those of BLT with large atom, La. Therefore, $\tau_{\varepsilon r}$ change to positive value with the substitution of small atoms on R site in $Ba_{6-x}R_{8+2x}Ti_{18}O_{54}$ is in consistent with the complex perovskite, where the $\tau_{\varepsilon r}$ also increases to positive value with the decrease of tolerance factor in the 3-tilt region.

4. Conclusion

1. The tilting and distortion of Ti-O octahedra and cation displacements in the pentagon-channel gave rise to the superlattice structure with a space group Pnam of doubled *c*-axis (*c*-axis ≈7.6 Å).

2. By refining the cation positions from the x-ray data and the oxygen from the neutron the most reliable refinement results was obtained in the aspect of the valence sum rule and calculated Ti-O bond lengths.

3. With the substitution of small size atom on the R-sites in $BaOR_2O_34TiO_2$ the crystal structure had more severely tilted and distorted octahedra. The $\tau_{\varepsilon r}$ of tungsten-bronze structure critically depends on the extent of the tilting and distortion of the octahedra in a similar manner to complex perovskite.

4. The dielectric properties of $\varepsilon_r = 89$–92, $Qf =$ 5855–6091 GHz are obtained in the range of $x \approx$ 0.04–0.08 in $BaO(Nd_{1-y}Bi_y)_2O_34TiO_2$. With Y-substitution dielectric properties of $\tau_{\varepsilon r} = +14$ ppm/°C and tan $\delta = 2 \times 10^{-3}$ were obtained at BaO $(Nd_{0.77}Y_{0.23})_2O_34TiO_2$ composition.

5. Suspected phase transitions are observed by DSC analysis in the temperature range of 280–310°C, and the heat anomaly was the most strong in $BaO(Nd_{0.77}Y_{0.23})_2O_34TiO_2$.

Acknowledgements

This work was supported by Korea Research Foundation, Project No. BSRI-97-2459. The authors appreciate the valuable assistance of Hyoun-Joo Kang in Dept. of Materials Engineering, Hoseo University.

References

1. K. WAKINO, T. NISHIGAWA, H. TAMURA and T. SUDO, *Microwave Journal* **6** (1987) 133.
2. D. KOLAR, Z. STADLER, S. GABERSCEK and D. SUVOROV, *Ber. Dtsh. Keram. Ges.* **55** (1978) 346.
3. H. OHSATO, T. OHHASHI, H. KATO, S. NISHIGAKI and T. OKUDA, *Jpn. J. Appl. Phys.* **34** (1995) 187.
4. J. TAKAHASHI, T. IKEGAMI and K. KAGEYAMA, *J. Amer. Ceram. Soc.* **74** (1991) 1868.
5. R. G. MATEEVA, M. B. VARFOLOMEEV and L. S. ILYUSCHENKO, *Russian J. of Inorganic Chemistry* **29** (1984) 17.
6. D. KOLAR, S. GABERSCEK and B. VOLAVSEK, *J. Solid State Chem.* **38** (1981) 158.
7. T. JAAKOLA, A. UUSIMAKI, R. RAUTIAHO and S. LEPPAVUORI, *J. Amer. Ceram. Soc.* **69** (1986) C-234.
8. F. AZOUGH, P. SETASUWON and R. FREER, in "Materials and Processes for Wireless Communications, Vol. 53," edited by T. Negas and H. Ling (1995 Ceramic Transaction) p. 215.
9. D. SUVOROV, M. VALANT, D. KOLA, *ibid.* p. 197.
10. H. OHSATO, S. NISHIGAKI and T. OKUDA, *Jpn. J. Appl. Phys.* **31** (1992) 3136.
11. P. LAFFEZ, G. DESGARDIN and B. RAVEAU, *J. of Mater. Sci.* **30** (1995) 267.
12. Z. M. DURAND and J. P. BOILOT, *J. Mat. Sci. Lett.* **6** (1987) 134.
13. W. WERSING, in "Electronic Ceramics," edited by B. C. H Steel (Elsevier, 1991) p. 67.
14. M. MIZUTA, K. UENOYAMA, H. OHSATO, S. NISHIGAKI and T. OKUDA, *Jpn. J. Appl. Phys.* **35** (1996) 5065.
15. R. D. SHANNON and C. T. PREWITT, *Acta Cryst.* **B25** (1969) 925.
16. B. W. HAKKI and P. D. COLEMAN, *IRE Trans. Microwave Theory and Tech.* **MTT-8** (1989) 402.
17. I. D. BROWN and D. ALTERMATT, *Acta Cryst.* **B41** (1985) 244.
18. E. L. COLLA, I. M. REANEY and N. SETTER, *J. Appl. Phys.* **74** (1993) 3414.
19. A. M. GLAZER, *Acta Cryst.* **A31** (1975) 756.

Received 29 October 1997
and accepted 24 August 1999